HHS Public Access

Author manuscript

*JACC Cardiovasc Imaging*. Author manuscript; available in PMC 2020 November 01.

Published in final edited form as:

*JACC Cardiovasc Imaging*. 2019 November ; 12(11 Pt 2): 2332–2344. doi:10.1016/j.jcmg.2019.06.031.

# Myocardial T1 and ECV Measurement:

## Underlying Concepts and Technical Considerations

**Austin A. Robinson, MD**[a], **Kelvin Chow, PhD**[b], **Michael Salerno, MD, PhD, MS**[a,c,d]

[a]Department of Medicine, Cardiovascular Division, University of Virginia Health System, Charlottesville, Virginia

[b]Siemens Medical Solutions USA, Inc., Chicago, Illinois

[c]Radiology and Medical Imaging, University of Virginia Health System, Charlottesville, Virginia

[d]Department of Biomedical Engineering, University of Virginia, Charlottesville, Virginia

## Abstract

Myocardial native T1 and extracellular volume fraction (ECV) mapping have emerged as cardiac magnetic resonance biomarkers providing unique insight into cardiac pathophysiology. Single breath-hold acquisition techniques, available on clinical scanners across multiple vendor platforms, have made clinical T1 and ECV mapping a reality. Although the relationship between changes in native T1 and alterations in cardiac microstructure is complex, an understanding of how edema, blood volume, myocyte and interstitial expansion, lipids, and paramagnetic substances affect T1 and ECV can provide insight into how and why these parameters change in various cardiac pathologies. The goals of this state-of-the-art review will be to review factors influencing native T1 and ECV, to describe how native T1 and ECV are measured, to discuss potential challenges and pitfalls in clinical practice, and to describe new T1 mapping techniques on the horizon.

### Keywords

cardiac magnetic resonance; extracellular volume (ECV); native T1

Over the past 2 decades, myocardial native T1 mapping and the assessment of extracellular volume fraction (ECV) by cardiac magnetic resonance (CMR) have developed into mature technologies that provide unique insights into cardiac pathophysiology (1). Although the concept of T1 mapping has existed for decades, rapid single breath-hold mapping techniques have made clinical CMR T1 mapping a reality (2-4). Although early clinical reports focused on using these metrics as a surrogate for quantifying diffuse myocardial fibrosis, our understanding of T1 and ECV has become more nuanced over time, and it is now recognized that these parameters can provide a richer characterization of the myocardium with sensitivity to numerous factors including edema, blood volume, myocyte expansion, ECV

**ADDRESS FOR CORRESPONDENCE:** Dr. Michael Salerno, Department of Medicine, Radiology, and Biomedical Engineering, Cardiovascular Division, University of Virginia Health System, 1215 Lee Street, P.O. Box 800158, Charlottesville, Virginia 22908, ms5pc@virginia.edu.

expansion secondary to protein infiltration, iron deposition, and intramyocardial lipids (5-9). This review will both describe the current state of the art of measurement techniques for myocardial T1 and ECV and discuss technical and physiological factors that affect native T1 and ECV. We will also review emerging techniques for T1 and ECV measurement, which have the potential to fundamentally alter how we make these measurements clinically.

## WHAT IS T1 MAPPING?

When a subject is placed in the CMR scanner, the proton spins, primarily from water and fat, orient either parallel or antiparallel to the main magnetic field, creating a net longitudinal magnetization aligned with the main magnetic field. This equilibrium magnetization can be perturbed with radiofrequency (RF) pulses used during imaging. Following an RF pulse, longitudinal magnetization recovers back to equilibrium exponentially, characterized by a recovery time constant denoted as T1.

The T1 recovery time can be spatially varying and depends on the local biochemical and molecular environment of the protons and, therefore, can be used to characterize variations in tissue composition. Images acquired at different times along the T1 recovery curve, which have a different T1 weighting, can be fit to an exponential recovery model describing T1 relaxation (10). The result is a quantitative map where each pixel's color represents the average T1 relaxation time within the voxel. This process is referred to as T1 mapping (Figure 1).

## WHAT FACTORS INFLUENCE NATIVE T1 OF THE MYOCARDIUM?

The sensitivity of native T1 to the local environment experienced by protons can be exploited to provide noninvasive soft-tissue characterization. In the realm of CMR, this can provide spatially resolved information characterizing myocardial pathology. To better understand what can be measured by T1 mapping, it is important to understand the factors that can affect the rate of longitudinal relaxation. Conditions that are favorable to energy transfer between the excited "spins" and their surroundings, the so-called "lattice," result in faster T1 relaxation times. This process is facilitated when molecules are tumbling at a rate close to the Larmor frequency or experience magnetic field fluctuations near the Larmor frequency. The Larmor frequency is the rate of precession of the protons at a given field strength. As a result, the T1 relaxation times will be longer at 3.0-T compared with 1.5-T because the Larmor frequency is proportional to the magnetic field strength.

Some generalizations can be made regarding molecular motion and myocardial T1. In tissues where water molecules are less restricted and move more freely, water has a higher tumbling rate and does not effectively undergo T1 relaxation, resulting in longer T1 relaxation times. This accounts for the longer T1 of blood and the higher myocardial native T1 in the presence of edema (11,12) (e.g., T1 mapping has been shown to have utility in the detection of edema in myocarditis) (13). In fact, a recent expert consensus recommends incorporation of T1 estimates for the evaluation of myocarditis (14). More broadly, this principle also accounts for higher native myocardial T1 in pathologies associated with

increases in the size of the ECV fraction such as in diseases characterized by myocardial fibrosis (15) or protein deposition as in amyloidosis (16,17).

On the other hand, slower moving protons in lipids in adipose tissue and cell membranes facilitate more effective T1 relaxation. This results in shorter T1 recovery times. Specific examples of short T1 tissues in CMR include lipomatous metaplasia after chronic myocardial infarction and sphingolipid accumulation resulting from Fabry disease and cardiac lipomas (9,18); however, a single voxel containing both intramyocardial fat and water will have 2 distinct T1 recovery curves and the measured T1 may be elevated or reduced, depending on the relative phase of the fat and water and the off-resonance frequency (19). Glycosphingolipid deposition in Fabry disease has a reported consistent T1 shortening, which may also be a result from the specific way that water is constrained, limiting water-lipid and water-proton interactions, similar to myelin in the brain (19).

T1 is also shortened in the presence of paramagnetic substances whose unpaired electrons cause large fluctuating local magnetic fields, enhancing the relaxation of nearby protons (20). The paramagnetic properties of certain oxidation states of iron account for the shortened T1 of water protons in the presence of iron (21). This can be seen in iron overload/siderosis and, more focally, in regions of intramyocardial hemorrhage in acute infarction. Although T2* has been more broadly studied for imaging iron overload, T1 mapping can also be useful in this regard because T1 and T2* are linearly related in the range of T2* values that are clinically relevant (22). Paramagnetic effects of iron in hemoglobin are also clinically relevant because T1 in the myocardium, as well as the blood pool, is reduced in the setting of anemia (23). As such, there is fairly linear relationship between the hemoglobin concentration of red blood cells and 1/T1 over a range of values, a phenomenon that may account for higher T1 times in women from the second through the fourth decades of life, presumably resulting from menstruation-related anemia (24,25). Super-paramagnetic iron nanoparticles have also been used at T1 shortening contrast agents (26,27). As will be discussed further on the section regarding ECV, possibly the most clinically relevant example of enhanced T1 relaxation resulting from paramagnetism is the effect of gadolinium-based contrast agents. Figure 2 summarizes how these different mechanisms contribute to the T1 relaxation properties of different tissues in various cardiac pathologies.

## CLINICAL UTILITY OF T1 MAPPING

The ability of T1 to provide myocardial tissue characterization has broad implications for the clinical realm, although an exhaustive discussion of their use is beyond the scope of this technical review. In addition to the states discussed here–edema, iron overload, protein infiltration, lipid deposition– myocardial T1 is altered across an array of conditions. These changes in T1 have diagnostic and prognostic utility. For example, left ventricular (LV) myocardial T1 is prolonged in valve disease, including aortic stenosis and mitral regurgitation, relative to healthy controls (28,29). T1 is elevated in both light-chain and transthyretin variants of cardiac amyloidosis (7,17). In a model of anthracycline-induced cardiotoxicity, myocardial T1 rises after chemotherapy exposures, albeit later than T2 (30). Vasodilator-induced changes in T1 have been used to detect obstructive coronary artery disease (see the section on Stress T1) (31). Furthermore, T1 of noninfarcted myocardium has

prognostic value in patients with known coronary artery disease (32). T1 is predictive of adverse events in nonischemic cardiomyopathy as well (33).

In addition, the relationship between T1 and hypertrophic cardiomyopathy (HCM), in which T1 has the potential to fill a needed role in risk stratification, is currently under study as part of the ongoing international hypertrophic cardiomyopathy registry (34).

## T1 MAPPING TECHNIQUES

### INVERSION RECOVERY APPROACHES.

There are several clinically available CMR pulse sequences for T1 mapping. The most widely disseminated strategy, modified Look-Locker inversion (MOLLI) recovery, involves the acquisition of single-shot diastolic images over successive heartbeats (typically 3 to 5) following an inversion RF pulse for T1 sensitization (Figure 1) (2). This scheme yields measurements along the T1 recovery curve at multiple inversion times that are separated by the R-R interval, termed a “Look-Locker set.” Following a rest period to allow the magnetization to recover toward equilibrium, additional Look-Locker sets with different inversion times may be used to better sample the T1 recovery curve. In the original implementation, there are 3 Look-Locker sets, with 3 images acquired in sequential RR intervals following each of the first 2 inversions pulses, and 5 following the third inversion pulse, with 3 resting heart beats between Look-Locker sets, denoted as 3(3) 3(3)5 (35). In this original technique, images are acquired over 17 heart beats. A limitation of this original implementation is the long breath-hold duration and sensitivity to heart rate resulting from incomplete recovery of magnetization between inversion pulses.

Variations of MOLLI have been proposed to reduce breath-hold duration and heart rate sensitivity. The shortened MOLLI technique (ShMOLLI) acquires 5 images following the first inversion and 2 additional images following acquired in a 5(1)1(1)1 scheme (3). With only a single heartbeat for recovery, tissues with long T1 do not experience complete magnetization recovery. A conditional processing technique is necessary to selectively discard images from later inversions to reduce T1 underestimation bias. This technique acquires data in 9 heartbeats and has been shown to be largely heart-rate independent (3). A 5(3) 3 sampling scheme is also commonly used and is insensitive to heart rate with a total acquisition time of 11 heartbeats (36). A 4(1)3(1)2 sampling scheme with shorter recovery durations may be used in postcontrast imaging because shorter T1 values recover to equilibrium more quickly (35). Currently, all major vendors have implementations of the MOLLI technique either available as a clinical product or as a research sequence.

Despite the popularity of the MOLLI technique, it has a number of potential limitations that can affect its accuracy and result in nonphysiologic variations in measured T1. The RF pulses used for image acquisition affect the recovery curve and cause a shortening in the apparent T1, termed T1*. A Look-Locker correction factor is commonly used to account for this effect, but is an approximation that is only strictly correct for continuous data acquisition with a low flip angle gradient echo technique following an inversion with complete recovery between inversion pulses (37). Second, the balanced steady-state free-precession readouts used for data acquisition introduce dependencies of the measured T1 on

a number of systematic confounders including the physiological dependencies on T2 relaxation and the magnetization transfer (MT), as well as nonphysiological dependencies on B1 (radiofrequency) and B0 (off-resonance) inhomogeneity and acquisition parameters, including the flip angle and repetition time (38). The physiological dependencies may increase the sensitivity of MOLLI T1 values to disease: increased T2 with edema and reduced MT effects in myocardial infarction increase MOLLI apparent T1 values. These confounders may result in reduced specificity and a systematic underestimation of the actual T1 relaxation time as measured by reference standard phantom measurements, trading accuracy for precision.

Despite these limitations, the MOLLI technique has been shown to be highly repeatable for a given set of sequence parameters, and the confounders of T2 and MT may increase its sensitive to pathology at the expense of reduced specificity to T1. MOLLI is also widely available, and relatively high precision in parametric maps improves visualization of focal disease; however, sensitivity to confounders have led the Society for Cardiovascular Magnetic Resonance (SCMR) consensus statement on parametric mapping to recommend using a fixed set of sequence parameters and using site-specific normal ranges (1). Several investigators have more accurately determined T1 using the MOLLI technique by using Bloch simulations that accurately describe the physics governing the expected magnetization T1 recovery, given the specific sequence parameters and timing (39,40).

## SATURATION RECOVERY.

An alternative approach to T1 mapping uses saturation recovery preparation pulses to null the net magnetization vector instead of inverting it. The prototypical SR technique is saturation recovery single-shot acquisition (SASHA), where 1 single-shot image is acquired without preparation and 10 images are acquired at different delays after saturation preparation (Figure 1). Unlike MOLLI-style sequences that acquire multiple images after a single preparation pulse, each SASHA image can be considered independently because each preparation pulse is followed by only a single image. This property affords SASHA insensitivity to heart rate, off-resonance, B1, T2, and magnetization transfer effects. The placement of both saturation and imaging modules in a single heartbeat limits the ability to acquire systolic data, however, which may be desirable for dilated cardiomyopathies, in which the myocardial walls are thin, or comparison to systolic first-pass perfusion data (see the section on Stress T1).

The saturation method using adaptive recovery times for cardiac T1 mapping ($SMART_1Map$) is a similar saturation-recovery T1 mapping technique. Unlike the SASHA sequence, in which saturation and imaging always occur within the same heartbeat, several images in $SMART_1Map$ have the saturation and imaging in separate heartbeats (41). This allows for the longer saturation times to be sampled, which may be advantageous for tissues with long T1. As a saturation recovery-based technique, phantom experiments demonstrated high accuracy of $SMART_1Map$, independent of heart rates and T1 time (42).

A limitation of saturation recovery techniques is their reduced dynamic range, which is effectively one-half of that in inversion recovery techniques (Figure 1). As a result, the saturation-recovery based SASHA has reduced T1 precision but increased accuracy

compared with the inversion-recovery based MOLLI (38). SASHA T1 values can also be biased in cases of low signal-to-noise ratio (SNR) and high heart rates limiting the maximum saturation recovery time if saturation and imaging are in the same RR. With a heart rate of 100 beats/min and an SNR of 20, <4% error is found in measurements of native myocardial T1 (38). T1 precision with SASHA data can be improved using a 2-parameter signal model, assuming ideal saturation that can be achieved with optimized saturation pulses (43). Improved precision from 2-parameter fitting is offset by a bias in T1 accuracy, but this can be substantially mitigated with the use of a variable flip-angle readout. Additional improvements in precision have also been proposed with numeric optimization of the saturation recovery times (44,45).

## T1 MAPPING: CLINICAL CONSIDERATIONS, CHALLENGES, AND PITFALLS

A critical requirement for the clinical use of T1 and ECV measurement is the establishment of normal reference ranges, at both 1.5- and 3.0-T field strengths (46). As noted in the recent SCMR consensus statement on parametric mapping, institution-specific normal ranges for native T1 should be established because the normal range of measured T1 values can depend on the field strength, vendor, pulse sequence, and specific pulse sequence parameters used. Local reference ranges and calibration are the most effective tools for addressing the limitations inherent in any of the mapping techniques discussed previously. As such, each institution with a reasonable volume of CMR should formalize T1 mapping protocols and use them as the basis for site-specific normal ranges. Importantly, any changes that a site implements in any aspect of their T1 analysis (e.g., sequence or postprocessing) should necessarily prompt a new evaluation of T1 normal values.

Generalized data can provide broad comparison but also underscore this point. A recent meta-analysis aggregating data from 120 publications and 5,541 healthy subjects found a pooled mean native T1 of 976 ms (95% confidence interval [CI]: 969 to 983 ms) at 1.5-T and 1,159 ms (95% CI: 1,143 to 1,175 ms) at 3.0-T for MOLLI-based pulse sequences (47). Importantly, there was a high degree of heterogeneity, with variations between vendors, MOLLI pulse sequence acquisition strategies, and sequence parameters including flip-angle and interinversion pulse delay. Although less extensively evaluated than MOLLI, normal native T1 values for SASHA have been reported between 1,149 and 1,202 ms (4,48,49).

Although vendor implementations of T1 mapping are largely automated, care should be taken to understand potential errors from technical failures. Pixel-wise T1 mapping relies on the accurate alignment of the individual T1-weighted source images and misalignment may result in T1 abnormalities that could be mistaken for pathology. Although motion correction techniques may generally be able to compensate for bulk respiratory motion from poor breath-holding, cardiac mistriggering is often uncorrectable. T1-weighted source images should be inspected as part of routine interpretation even if motion correction is used, with the objective of identifying uncorrected residual motion or distortions from failures in motion correction.

Care must also be taken in the clinical interpretation of mildly abnormal native T1 values, keeping in mind the measurement uncertainty and the clinical context of the study. A study

comparing myocardial native T1 data from 1,291 clinical scans across 16 cardiovascular pathologies and 342 healthy volunteers, all performed at a single center and using ShMOLLI-based mapping technique demonstrated that only 3 conditions had statistically different T1 values from the normal range (50). These conditions were Fabry disease and iron overload (low T1) and cardiac amyloidosis (high T1). Again, sequence is an important consideration as all T1 estimates were performed with ShMOLLI. There are no similar studies using SASHA or MOLLI for context.

## WHAT IS ECV MAPPING AND HOW IS IT PERFORMED?

The myocardium has a complex microstructure consisting of intracellular space, made up of cells including myocytes, fibroblasts, blood vessel walls, and cells within blood, and an extracellular space composed of the plasma space, and the extravascular interstitial space (Central Illustration). Gadolinium-based contrast agents are extracellular agents that do not enter the intracellular space. Following its intravenous injection, gadolinium contrast agent is distributed only within the extracellular volume. Assuming a single compartment or fast exchange between multiple compartments, the concentration of gadolinium (Gd) contrast agent can be estimated by the change in T1 value and the relaxivity of the contrast agent (51,52):

$$[Gd] = \left(\frac{1}{T1_{post}} - \frac{1}{T1_{pre}}\right) \Big/ r \qquad \text{[Equation 1]}$$

The contrast concentration in the myocardium can be normalized to the concentration in the blood to yield the partition coefficient ($\lambda$):

$$\lambda = \frac{[Gd]_{myo}}{[Gd]_{blood}} \qquad \text{[Equation 2]}$$

Because the contrast agent is extracellular, it also does not enter into the intracellular space of the red blood cells within the blood pool. Applying a correction factor for the hematocrit (Hct), the extracellular volume can be estimated as:

$$ECV = (1 - Hct) \bullet \lambda = (1 - Hct) \frac{\left(\frac{1}{T1_{myo\ post}} - \frac{1}{T1_{myo\ pre}}\right)}{\left(\frac{1}{T1_{blood\ post}} - \frac{1}{T1_{blood\ pre}}\right)} \qquad \text{[Equation 3]}$$

After the intravenous injection of contrast into the body, its concentration within the myocardium and blood change continuously because of perfusion and contrast agent clearance by the renal system. An accurate estimate of the ECV necessitates the relative concentrations in the myocardium and blood be in equilibrium. Early approaches to T1-based ECV estimation used a bolus of contrast followed by a slow infusion of contrast agent (53). If, however, measurements are taken following a sufficiently long delay such that

perfusion effects can be neglected, the concentration of gadolinium in the blood pool and interstitium are changing slowly enough such that their ratio is approximately constant (53,54). This dynamic equilibrium is generally assumed to be established 10 min after contrast agent administration (1) and ECV measurements taken after this time have similar accuracy to the continuous infusion approach (55,56). The assumption of dynamic equilibrium can be verified by taking multiple post-contrast T1 measurements at various times. Because the ratio of contrast concentrations in blood to tissue is constant during the dynamic equilibrium phase, the partition coefficient can be determined as the slope of the line generated by plotting R1 = 1/T1 measurements in the myocardium against those in the bloodpool. Nonlinearity in the relationship between blood and tissue relaxation rates may be the result of intermediate or slow exchange between intracellular and interstitial spaces and has been used to characterize myocyte size (57); however, because this requires multiple measurements, it is often not performed in clinical practice. Single post-contrast T1 measurement 10 min following contrast injection is typically clinically sufficient (1).

## WHAT FACTORS INFLUENCE MYOCARDIAL ECV?

ECV mapping has advantages over late gadolinium enhancement (LGE) imaging of fibrosis in that it is intrinsically quantitative and can assess both focal and diffuse fibrosis (36). Although fibrosis is certainly a cause of increased ECV, it is not the only cause. Expansion of the interstitial space may also occur from diffuse protein deposition (as in amyloid) or edema (35). Changes in vascular volume can affect ECV estimates as well (see the section on Stress T1). Finally, it should be kept in mind that ECV is a volume fraction, so that it can be changed indirectly via changes in size of the intracellular volume. For example, in hypertensive LV hypertrophy, there is an expansion of both the myocyte volume resulting from myocyte hypertrophy (intracellular) as well as the interstitial space resulting from fibrosis (extracellular); however, the expansion of the interstitial space is greater, resulting in a relative increase in ECV (58). In contrast, in athletic hypertrophy, the expansion is primarily the result of cellular hypertrophy; consequently, the ECV is decreased (6). These influences on the ECV are depicted in Figure 3.

## CLINICAL UTILITY OF ECV MAPPING

The opposite directionality of ECV in different states–decreased in athletic remodeling, but increased in HCM–provides a straightforward mechanism for discriminating between 2 otherwise phenotypically similar entities. Of importance, this simple distinction has the potential to spare patients the costly and time-consuming process of athletic detraining. ECV mapping has clinical utility beyond HCM as well. ECV elevations precede the development of LGE in cardiac amyloid, allowing for diagnosis at earlier disease stages (59). ECV is also prognostic in amyloid, with 1 study reporting a hazard ratio of death of 3.85 for ECV fractions >45% (60). In valvular heart disease, elevations in ECV, but not T1 or LGE, in aortic and mitral valve disease correlate well with histologic fibrosis and, at least in aortic stenosis, track well with cardiac decompensation (61,62). Further, myocardial fibrosis in aortic regurgitation appears to be a significant predictor of LV ejection fraction after valve replacement (63). The suggestion that ECV mapping could inform timing of aortic valve replacement is particularly intriguing, given recent evidence questioning the adequacy of

current guidelines regarding use of LV indexed end-systolic diameter to guide surgical candidacy (64).

## ECV MAPPING: CLINICAL CONSIDERATIONS, CHALLENGES, AND PITFALLS

Several technical factors can affect ECV assessment. Foremost, any errors or biases in T1 measurements will be propagated through to ECV estimates. Because the changes in T1 are reliant on gadolinium contrast agent kinetics and distribution, protocol conditions should be standardized and consistently followed, including a consistent method and dosage of gadolinium administration. Gadolinium may be administered via continued infusion or bolus, so long as time is provided to achieve dynamic equilibrium as described previously (55,56). For bolus administration, the SCMR consensus statement recommends at least 10 min be allowed after gadolinium bolus before acquisition of post-contrast T1 images. Also per guidelines, protein-bound gadolinium contrast agents, such as gadobenate dimeglumine, should be avoided because they have a different volume of distribution and will thus affect ECV measurements (1). Just as the components of the partition coefficient (T1 and gadolinium) can affect ECV, so can errors involving determination of the plasma volume fraction (1 – Hct). Every effort should be taken to ensure the accuracy of the hematocrit, including phlebotomy as close as possible to the time of CMR examination and standardization in its relative timing (65). Care should be taken in using alternatives to laboratory measurement of blood hematocrit as well. So-called “synthetic” hematocrit assessments use the near-linear relationship between the T1 relaxation rate of blood ($1/T1_{blood}$) and hematocrit to estimate blood hematocrit at the time of scan (24); however, there is some concern about the introduction of additional error with this approach. For example, a single-institution study suggested that synthetic hematocrit results in smaller ECV values >30.5% leading to significantly lower estimates of ECV in patients with HCM and in a diagnostic model, would incorrectly classify 8% to 18% of patients with HCM as having normal ECV (66).

As with native T1, understanding ECV reference ranges is of paramount importance. A recent meta-analysis of normal values for ECV pooled 81 publications and 3,872 subjects with ECV measurements and found the pooled mean was 25.9% (95% CI: 25.2% to 26.3%) at 1.5 Tesla and 25.9% (95% CI: 25.4% to 26.5%) at 3T (47). Thus, unlike native T1, which is field-strength dependent, ECV is relatively field-strength independent, as would be expected based on its definition. However, $\lambda$ and ECV values vary with T1 mapping technique, and although ECV has been well correlated with histological measures of collagen volume fraction, absolute accuracy of T1-derived ECV measures is less well validated (38,53,67,68).

Software and workflow advances are aiding the inclusion of ECV measurement in routine clinical care. The equation for ECV calculation is relatively straightforward and could in principle be done manually during postprocessing. Such global ECV measurements can be performed by identifying the average native and postcontrast T1 over a myocardial region of interest and then using these values, along with a hematocrit, to provide a global averaged

ECV. By contrast, vendors are increasingly including postprocessing software capable of generating ECV maps, based on the pixel-wise native and post-contrast T1 values, provided they are of matching slice location and cardiac phase. As discussed for T1 mapping, care should be taken to ensure the high quality of ECV maps. For pixel-wise ECV maps, native and postcontrast T1 maps must be correctly aligned to avoid errors, and automatic image registration should be carefully inspected for residual motion. Because ECV maps are determined from 2 T1 maps and a hematocrit measurement, which all have some degree of uncertainty, the errors in these individual measurements will propagate into ECV, leading to a greater uncertainty in this parameter.

## EMERGING METHODS

### WHOLE HEART COVERAGE, FREE-BREATHING, AND 3-DIMENSIONAL T1 MAPPING.

In practice, T1 and ECV maps are often acquired in 1 to 3 short-axis slices and potentially a single long-axis slice of the LV. Such limited coverage has the potential to miss focal segments of pathology. Consequently, there is a desire to provide whole heart coverage with quantitative T1 mapping. This clinical need has in-turn motivated the development of intrinsically multislice and 3-dimensional (3D) techniques (69). In the slice-interleaved T1 (STONE) approach, 5 short-axis slices are acquired with single-shot imaging in 5 consecutive heartbeats after a single inversion pulse. After a rest period, the scheme is repeated with the order of the short-axis slices, resulting in each slice being acquired with 5 different inversion times separated by multiples of the subject's R-R interval. Noninverted images are also acquired at each slice. Acquisitions are performed in free-breathing with prospective slice tracking. STONE is appealing because of its efficient multislice coverage; however, blood T1 measurements may be unreliable because of inflow effects, limiting its use for ECV mapping (70). STONE also remains susceptible to T1 underestimation from B1 heterogeneity and has not been well validated clinically.

The SASHA sequence has recently been extended to a free-breathing acquisition using image-based motion correction averaging (48). Because of the saturation-recovery nature of SASHA, individual images are independent and can be discarded without consideration of magnetization history. Poor intrinsic blood-tissue contrast in the SASHA images necessitated a modification of the imaging acquisition to generate images with sufficient blood-tissue contrast for robust image registration. Myocardial T1 values with free-breathing SASHA were similar to conventional breath-hold SASHA, with a precision equivalent to that of MOLLI for acquisitions approximately 30 s in duration; however, the technique has not been extensively validated, particularly for long-axis slice orientations in which through-plane motion cannot be remediated with retrospective image-based motion correction.

Intrinsically, 3D acquisitions are appealing because of their increased SNR, gapless spatial coverage, and simplicity of planning. Because of the increased k-space sampling required for 3D imaging, segmented acquisitions are used instead of single-shot acquisitions popular in 2-dimensional (2D) imaging. Because image-based motion correction is not possible with segmented imaging, 3D techniques assume no motion during breath-holds or rely on other forms of respiratory motion compensation such as a respiratory navigator. Other tradeoffs inherent in the move from 2D to 3D mapping, such as potential reduction of in-plane spatial

resolution to reduce scan times and T1 accuracy or precision, must be well characterized before 3D imaging is widely accepted.

The accelerated and navigator-gated look-locker imaging for cardiac T1 estimation (ANGIE) technique is an extension of the MOLLI approach using a segmented acquisition with navigator gating (69,71). ANGIE uses MOLLI-like Look-Locker acquisitions and a compressed sensing reconstruction algorithm to acquire high-resolution ($1.2 \times 1.2$ mm$^2$) 2D T1 maps. The technique has also been extended to 3D volumetric ($1.4 \times 1.4 \times 4$ mm$^3$) T1 maps with an acquisition time of <7 min. ANGIE T1 values were similar to MOLLI, but with reduced precision resulting from higher resolution and reduced number of acquired images. Although promising, ANGIE awaits clinical validation.

Three-dimensional quantification using an interleaved Look-Locker acquisition sequence with T2-preparation (QALAS) is a simultaneous T1 and T2 mapping technique combining inversion and T2 preparation pulses (72). To acquire the necessary data in a single breath-hold, only 5 points are acquired along a combined T2 prepared and inversion recovery curve. In contrast to the least squares fitting used in conventional T1 mapping techniques, measured signal intensities are fit to a simulation of magnetization evolution following the preparation pulses. This simulation-based approach can potentially overcome the reduced intrinsic SNR from the small number of sampled data points and the low 5° flip angle. The precision of 3D-QALAS has yet to be systematically evaluated relative to conventional mapping techniques, however, and assumptions made in the simulation could introduce systematic errors.

SASHA is amenable to segmented acquisitions because of its fixed saturation-recovery times, compared with the heart rate-dependent inversion recovery times of MOLLI-like techniques. The recently proposed 3D SASHA is a segmented acquisition approach for T1 mapping acquired during free-breathing with prospective motion correction using a diaphragmatic navigator (73). With a moderately high in-plane resolution of $1.4 \times 1.4$ mm$^2$, total acquisition time was reported to be approximately 12 min. Myocardial T1 values with 3D SASHA were similar to 2D SASHA, suggesting similar robustness to confounders with improved precision. Although 3D SASHA has an improved slice partition thickness of 8 mm compared with 12 mm of 3D QALAS, both techniques are still highly spatially anisotropic. Further improvements in slice resolution with these techniques or with non-Cartesian trajectories may enable quantitative mapping complex structures such as the right ventricle or left atrium.

## MODEL-BASED PARAMETRIC MAPPING.

Conventional T1 mapping techniques acquire multiple images at various inversion or saturation recovery times that can be fit to an exponential recovery curve. In contrast, the recently introduced MRI fingerprinting techniques do not acquire individual images, but rather use a Bloch equation simulation to model the signal evolution following preparation pulses at each pixel location (74). By using a highly undersampled fast imaging with steady precession-based spiral pulse sequence with continually varying sequence parameters such as flip angle and TR, tissues with different T1s and T2s will have unique signal evolutions (i.e., “fingerprints”) that can be matched to a dictionary of signal evolutions based on the

exact acquisition parameters for a given T1 and T2. For CMR fingerprinting, a few modifications are used (75). The acquisition is performed during a breath-hold using electrocardiogram gating, with inversion or T2 preparation pulses added for increased sensitivity. The specific evolution of signal including the patient-specific sequence timing because of the patient's exact heart rate are simulated. Initial data show similar myocardial and blood T1 values to MOLLI, with comparable quality T1 and T2 maps. Alternatively, emerging model-based methods of parametric mapping that use Bloch simulations, such as SQUAREMR, are being used to estimate magnetization recovery and thus T1, with existing sequences (39). Ongoing work with CMR fingerprinting and SQUAREMR includes improvements to accuracy and robustness and clinical validation (76).

Another recent technique called CMR multitasking can acquire cardiac T1 maps during a nongated free breathing acquisition (77). This technique relies on the assumption that respiratory motion, cardiac motion, and T1 recovery can each be approximated by a small number of basis functions. Using a mathematical technique called low-rank tensor factorization, ungated data binned according to inversion time and respiratory and cardiac phase can be jointly reconstructed so that images can be displayed at any combination of inversion time, cardiac cycle, and respiratory position. Myocardial T1 values with multitasking were similar to MOLLI, with higher coefficient of variation for repeated T1 measures but lower coefficient of variation for ECV. These emerging model-based techniques have the potential to accelerate acquisitions and improve robustness to motion, but further work is still required to establish their overall performance relative to existing techniques.

### STRESS T1.

A new potential use for T1 mapping has come from its application to the diagnosis of obstructive coronary artery disease. Stress testing with T1 mapping takes advantage of myocardial blood volume changes distal to coronary stenoses, specifically the higher myocardial blood volume at rest and limited increase in volume with vasodilation (62). The difference between vasodilator-stress and resting T1 values, termed the T1 reactivity, is able to effectively distinguish between ischemic, infarcted, and remote myocardial segments (5,31); however, the diagnostic performance of stress T1 seems to be significantly reduced when performed without using visual contrast-enhanced perfusion defects to select focal regions for analysis (78). Multicenter studies are needed to validate this promising noncontrast technique for diagnosing obstructive coronary lesions.

## CONCLUSIONS

T1 and ECV mapping are now established techniques that can provide unique insight into various pathological myocardial processes (Central Illustration). These techniques have entered routine clinical practice, and data continue to emerge regarding diagnostic and prognostic utility. MOLLI-based pulse sequences are becoming widely available, and care must be exercised to make sure that T1 mapping and ECV techniques are being applied appropriately to maximize clinical utility. Clinical guidance regarding best practices have been delineated in an SCMR consensus statement on parametric mapping. For the detection

of focal pathology, T1 and T2 mapping techniques may be able replace older dark-blood fast spin echo-based T1 and T2 weighted techniques. For diffuse processes, T1 and ECV mapping techniques need to be applied carefully in the context of the uncertainty in these parameters. Native T1 and ECV are markedly increased in the presence of cardiac amyloidosis, and native T1 is markedly reduced in Fabry disease and iron overload. Emerging techniques promise improved T1 mapping techniques with high-resolution and improved spatial coverage, and free-breathing nongated techniques are on the horizon. Stress T1 mapping may provide novel insights into abnormalities in vascular tone in coronary artery disease and microvascular disease. T1 and ECV mapping techniques have become mature clinically relevant CMR biomarkers.

## Acknowledgments

Funding sources include National Institutes of Health grants R01 HL131919 and T32 EB003841. Dr. Chow is an employee of Siemens Medical Solutions USA, Inc. Dr. Salerno has received research support from Siemens Medical Solutions USA, Inc. Dr. Robinson has reported that he has no relationships relevant to the contents of this paper to disclose.

## ABBREVIATIONS AND ACRONYMS

| | |
|---|---|
| **2D** | 2-dimensional |
| **3D** | 3-dimensional |
| **ANGIE** | accelerated and navigator-gated look-locker imaging for cardiac T1 estimation |
| **CI** | confidence interval |
| **CMR** | cardiac magnetic resonance |
| **ECV** | extracellular volume |
| **HCM** | hypertrophic cardiomyopathy |
| **Hct** | hematocrit |
| **LV** | left ventricular |
| **LGE** | late gadolinium enhancement |
| **MOLLI** | modified Look-Locker inversion recovery |
| **MT** | magnetization transfer |
| **QALAS** | quantification using an interleaved Look-Locker acquisition sequence with T2-preparation |
| **RF** | radiofrequency |
| **SASHA** | saturation recovery single-shot acquisition |
| **SCMR** | Society for Cardiovascular Magnetic Resonance |

| | |
|---|---|
| **ShMOLLI** | shortened modified Look-Locker inversion recovery technique |
| **SMART$_1$Map** | saturation method using adaptive recovery times for cardiac T1 mapping |
| **SNR** | signal-to-noise ratio |
| **STONE** | slice-interleaved T1 |

## REFERENCES


1. MessroghLi DR, Moon JC, Ferreira VM, et al. Clinical recommendations for cardiovascular magnetic resonance mapping of T1, T2, T2* and extraceLLuLar voLume: a consensus statement by the Society for CardiovascuLar Magnetic Resonance (SCMR) endorsed by the European Association for CardiovascuLar Imaging (EACVI). J Cardiovasc Magn Res 2017;19:75.
2. MessroghLi DR, Radjenovic A, Kozerke S, Higgins DM, Sivananthan MU, Ridgway JP. Modified Look-Locker inversion recovery (MOLLI) for high-resoLution T1 mapping of the heart. Magn Res Med 2004;52:141.
3. Piechnik SK, Ferreira VM, Dall'Armellina E, et al. Shortened modified Look-Locker inversion recovery (ShMOLLI) for clinical myocardial T1-mapping at 1.5 and 3 T within a 9 heartbeat breathhold. J Cardiovasc Magn Res 2010;12:69.
4. Chow K, Flewitt JA, Green JD, Pagano JJ, Friedrich MG, Thompson RB. Saturation recovery single-shot acquisition (SASHA) for myocardial T1 mapping. Magn Res Med 2014;71:2082.
5. Liu A, Wijesurendra RS, Francis JM, et al. Adenosine stress and rest T1 mapping can differentiate between ischemic, infarcted, remote, and normal myocardium without the need for gadolinium contrast agents. J Am Coll Cardiol Img 2016;9:27.
6. Swoboda PP, McDiarmid AK, Erhayiem B, et al. Assessing myocardial extracellular volume by T1 mapping to distinguish hypertrophic cardiomyopathy from athlete's heart. J Am Coll Cardiol 2016; 67:2189. [PubMed: 27151352]
7. Fontana M, Banypersad SM, Treibel TA, et al. Native T1 mapping in transthyretin amyloidosis. J Am Coll Cardiol Img 2014;7:157.
8. Sado DM, Maestrini V, Piechnik SK, et al. Noncontrast myocardial T1 mapping using cardiovascular magnetic resonance for iron overload. J Magnet Res Img 2015;41:1505.
9. Sado DM, White SK, Piechnik SK, et al. Identification and assessment of Anderson-Fabry disease by cardiovascular magnetic resonance noncontrast myocardial T1 mapping. Circ Cardiovasc Img 2013;6:392.
10. Taylor AJ, Salerno M, Dharmakumar R, Jerosch-Herold M. T1 mapping: basic techniques and clinical applications. J Am Coll Cardiol Img 2016;9: 67.
11. Messroghli DR, Niendorf T, Schulz-Menger J, Dietz R, Friedrich MG. T1 mapping in patients with acute myocardial infarction: myocardial infarction and scar. J Cardiovasc Magn Res 2003;5:353.
12. Ugander M, Bagi PS, Oki AJ, et al. Myocardial edema as detected by pre-contrast T1 and T2 CMR delineates area at risk associated with acute myocardial infarction. J Am Coll Cardiol Img 2012; 5:596.
13. Pan JA, Lee YJ, Salerno M. Diagnostic performance of extracellular volume, native T1, and T2 mapping versus Lake Louise Criteria by cardiac magnetic resonance for detection of acute myocarditis: a meta-analysis. Circ Cardiovasc Img 2018;11:e007598.
14. Ferreira VM, Schulz-Menger J, Holmvang G, et al. Cardiovascular magnetic resonance in nonischemic myocardial inflammation: expert recommendations. J Am Coll Cardiol 2018;72:3158. [PubMed: 30545455]
15. Hinojar R, Varma N, Child N, et al. T1 mapping in discrimination of hypertrophic phenotypes: hypertensive heart disease and hypertrophic cardiomyopathy: findings from the International T1 Multicenter Cardiovascular Magnetic Resonance Study. Circ Cardiovasc Img 2015;8.
16. Brooks J, Kramer CM, Salerno M. Markedly increased volume of distribution of gadolinium in cardiac amyloidosis demonstrated by T1 mapping. J Magnet Res Img 2013;38:1591.

17. Karamitsos TD, Piechnik SK, Banypersad SM, et al. Noncontrast T1 mapping for the diagnosis of cardiac amyloidosis. J Am Coll Cardiol Img 2013;6: 488.
18. Maleszewski JJ, Bois MC, Bois JP, Young PM, Stulak JM, Klarich KW. Neoplasia and the heart: pathological review of effects with clinical and radiological correlation. J Am Coll Cardiol 2018;72:202. [PubMed: 29976295]
19. Kellman P, Bandettini WP, Mancini C, Hammer-Hansen S, Hansen MS, Arai AE. Characterization of myocardial T1-mapping bias caused by intramyocardial fat in inversion recovery and saturation recovery techniques. J Cardiovasc Magn Res 2015; 17:33.
20. De León-Rodríguez LM, Martins AF, Pinho MC, Rofsky NM, Sherry AD. Basic MR relaxation mechanisms and contrast agent design. J Magnet Res Img 2015;42:545.
21. White DL. Paramagnetic iron (III) MRI contrast agents. Magn Res Med 1991;22:309.
22. Feng Y, He T, Carpenter JP, et al. In vivo comparison of myocardial T1 with T2 and T2* in thalassaemia major. J Magnet Res Img 2013;38:588.
23. Spees WM, Yablonskiy DA, Oswood MC, Ackerman JJH. Water proton MR properties of human blood at 1.5 Tesla: magnetic susceptibility, T1, T2, T, and non-Lorentzian signal behavior. Magn Res Med 2001;45:533.
24. Treibel TA, Fontana M, Maestrini V, et al. Automatic measurement of the myocardial interstitium: synthetic extracellular volume quantification without hematocrit sampling. J Am Coll Cardiol Img 2016;9:54.
25. Piechnik SK, Ferreira VM, Lewandowski AJ, et al. Normal variation of magnetic resonance T1 relaxation times in the human population at 1.5 T using ShMOLLI. J Cardiovasc Magn Res 2013;15:13.
26. Wang Y-XJ, Hussain SM, Krestin GP. Super-paramagnetic iron oxide contrast agents: physicochemical characteristics and applications in MR imaging. Eur Radiol 2001;11:2319. [PubMed: 11702180]
27. Li W, Tutton S, Vu AT, et al. First-pass contrast-enhanced magnetic resonance angiography in humans using ferumoxytol, a novel ultrasmall superparamagnetic iron oxide (USPIO)-based blood pool agent. J Magnet Res Img 2005; 21:46.
28. Lee H, Park J-B, Yoon YE, et al. Noncontrast myocardial T1 mapping by cardiac magnetic resonance predicts outcome in patients with aortic stenosis. J Am Coll Cardiol Img 2018;11:974–83.
29. Pradella S, Grazzini G, Brandani M, et al. Cardiac magnetic resonance in patients with mitral valve prolapse: Focus on late gadolinium enhancement and T1 mapping. Eur Radiol 2019; 29:1546–54. [PubMed: 30088066]
30. Galán-Arriola C, Lobo M, Vílchez-Tschischke JP, et al. Serial magnetic resonance imaging to identify early stages of anthracycline-induced cardiotoxicity. J Am Coll Cardiol 2019; 73:779–91. [PubMed: 30784671]
31. Liu A, Wijesurendra RS, Liu JM, et al. Gadolinium-free cardiac MR stress T1-mapping to distinguish epicardial from microvascular coronary disease. J Am Coll Cardiol 2018;71:957. [PubMed: 29495995]
32. Puntmann VO, Carr-White G, Jabbour A, et al. Native T1 and ECV of noninfarcted myocardium and outcome in patients with coronary artery disease. J Am Coll Cardiol 2018;71:766–78. [PubMed: 29447739]
33. Puntmann VO, Carr-White G, Jabbour A, et al. T1-mapping and outcome in nonischemic cardiomyopathy: all-cause mortality and heart failure. J Am Coll Cardiol Img 2016;9:40–50.
34. Kramer CM, Appelbaum E, Desai MY, et al. Hypertrophic Cardiomyopathy Registry: the rationale and design of an international, observational study of hypertrophic cardiomyopathy. Am Heart J 2015;170:223. [PubMed: 26299218]
35. Kellman P, Hansen MS. T1-mapping in the heart: accuracy and precision. J Cardiovasc Magn Res 2014;16:2.
36. Ugander M, Oki AJ, Hsu L-Y, et al. Extracellular volume imaging by magnetic resonance imaging provides insights into overt and sub-clinical myocardial pathology. Eur Heart J 2012;33:1268. [PubMed: 22279111]

37. Deichmann R, Haase A. Quantification of T1 values by SNAPSHOT-FLASH NMR imaging. J Magn Res (1969) 1992;96:608.
38. Roujol S, Weingartner S, Foppa M, et al. Accuracy, precision, and reproducibility of four T1 mapping sequences: a head-to-head comparison of MOLLI, ShMOLLI, SASHA, and SAPPHIRE. Radiology 2014;272:683. [PubMed: 24702727]
39. Xanthis CG, Bidhult S, Kantasis G, Heiberg E, Arheden H, Aletras AH. Parallel simulations for QUAntifying RElaxation magnetic resonance constants (SQUAREMR): an example towards accurate MOLLI T1 measurements. J Cardiovasc Magn Res 2015;17:104.
40. Shao J, Rapacchi S, Nguyen KL, Hu P. Myocardial T1 mapping at 3.0 tesla using an inversion recovery spoiled gradient echo readout and bloch equation simulation with slice profile correction (BLESSPC) T1 estimation algorithm. J Magnet Res Img 2016;43:414.
41. Slavin GS, Hood MN, Ho VB, Stainsby JA. Breath-held myocardial T1 mapping using multiple single-point saturation recovery. Proc ISMRM 2012:1244.
42. Stainsby JA, Slavin GS. Comparing the accuracy and precision of SMART1Map, SASHA and MOLLI. J Cardiovasc Magn Res 2014;16:P11.
43. Chow K, Kellman P, Spottiswoode BS, et al. Saturation pulse design for quantitative myocardial T 1 mapping. J Cardiovasc Magn Res 2015;17: 84.
44. Kellman P, Xue H, Chow K, Spottiswoode BS, Arai AE, Thompson RB. Optimized saturation recovery protocols for T1-mapping in the heart: influence of sampling strategies on precision. J Cardiovasc Magn Res 2014;16:55.
45. Akçakaya M, Weingärtner S, Roujol S, Nezafat R. On the selection of sampling points for myocardial T1 mapping. Magn Res Med 2015;73: 1741.
46. Kawel-Boehm N, Maceira A, Valsangiacomo-Buechel ER, et al. Normal values for cardiovascular magnetic resonance in adults and children. J Cardiovasc Magn Res 2015;17:29.
47. Gottbrecht M, Kramer CM, Salerno M. Native T1 and extracellular volume measurements by cardiac MRI in healthy adults: a meta-analysis. Radiology 2018:180226.
48. Chow K, Yang Y, Shaw P, Kramer CM, Salerno M. Robust free-breathing SASHA T 1 mapping with high-contrast image registration. J Cardiovasc Magn Res 2016;18:47.
49. Pagano JJ, Chow K, Paterson DI, et al. Effects of age, gender, and risk-factors for heart failure on native myocardial T1 and extracellular volume fraction using the SASHA sequence at 1.5 T. J Magnet Res Img 2018;48:1307–17.
50. Liu JM, Liu A, Leal J, et al. Measurement of myocardial native T1 in cardiovascular diseases and norm in 1291 subjects. J Cardiovasc Magn Res 2017;19:74.
51. Hk Arheden, Saeed M Higgins CB, et al. Measurement of the distribution volume of gadopentetate dimeglumine at echo-planar MR imaging to quantify myocardial infarction: comparison with 99mTc-DTPA autoradiography in rats. Radiology 1999;211:698. [PubMed: 10352594]
52. Donahue KM, Weisskoff RM, Burstein D. Water diffusion and exchange as they influence contrast enhancement. J Magnet Res Img 1997;7:102–10.
53. Flett AS, Hayward MP, Ashworth MT, et al. Equilibrium contrast cardiovascular magnetic resonance for the measurement of diffuse myocardial fibrosis: preliminary validation in humans. Circulation 2010;122:138. [PubMed: 20585010]
54. Jerosch-Herold M, Sheridan DC, Kushner JD, et al. Cardiac magnetic resonance imaging of myocardial contrast uptake and blood flow in patients affected with idiopathic or familial dilated cardiomyopathy. Am J Physiol 2008;295:H1234.
55. Schelbert EB, Testa SM, Meier CG, et al. Myocardial extravascular extracellular volume fraction measurement by gadolinium cardiovascular magnetic resonance in humans: slow infusion versus bolus. J Cardiovasc Magn Res 2011;13:16.
56. Salerno M, Janardhanan R, Jiji RS, et al. Comparison of methods for determining the partition coefficient of gadolinium in the myocardium using T1 mapping. J Magnet Res Img 2013; 38:217.
57. Coelho-Filho OR, Shah RV, Mitchell R, et al. Quantification of cardiomyocyte hypertrophy by cardiac magnetic resonance: implications for early cardiac remodeling. Circulation 2013;128:1225–33. [PubMed: 23912910]

58. Kuruvilla S, Janardhanan R, Antkowiak P, et al. Increased extracellular volume and altered mechanics are associated with LVH in hypertensive heart disease, not hypertension alone. J Am Coll Cardiol Img 2015;8:172.
59. Fontana M, Pica S, Reant P, et al. Prognostic value of late gadolinium enhancement cardiovascular magnetic resonance in cardiac amyloidosis. Circulation 2015;132:1570–9. [PubMed: 26362631]
60. Banypersad SM, Fontana M, Maestrini V, et al. T1 mapping and survival in systemic light-chain amyloidosis. Eur Heart J 2014;36:244–51. [PubMed: 25411195]
61. de Ravenstein CdM, Bouzin C, Lazam S, et al. Histological validation of measurement of diffuse interstitial myocardial fibrosis by myocardial extravascular volume fraction from Modified Look-Locker imaging (MOLLI) T1 mapping at 3 T. J Cardiovasc Magn Res 2015;17:48.
62. Chin CW, Everett RJ, Kwiecinski J, et al. Myocardial fibrosis and cardiac decompensation in aortic stenosis. J Am Coll Cardiol Img 2017;10: 1320–33.
63. De Meester C, Boileau L, Roy C, et al. The role of fibrosis on the postoperative LV function in severe aortic regurgitation. Arch Cardiovasc Dis Suppl 2018;10:218.
64. Yang L-T, Michelena HI, Scott CG, et al. Outcomes in chronic hemodynamically significant aortic regurgitation and limitations of current guidelines. J Am Coll Cardiol 2019;73:1741–52. [PubMed: 30846339]
65. Engblom H, Kanski M, Kopic S, et al. Importance of standardizing timing of hematocrit measurement when using cardiovascular magnetic resonance to calculate myocardial extracellular volume (ECV) based on pre-and post-contrast T1 mapping. J Cardiovasc Magn Res 2018;20:46.
66. Shang Y, Zhang X, Zhou X, Wang J. Extracellular volume fraction measurements derived from the longitudinal relaxation of blood-based synthetic hematocrit may lead to clinical errors in 3 T cardiovascular magnetic resonance. J Cardiovasc Magn Res 2018;20:56.
67. Fontana M, White SK, Banypersad SM, et al. Comparison of T1 mapping techniques for ECV quantification. Histological validation and reproducibility of ShMOLLI versus multibreath-hold T1 quantification equilibrium contrast CMR. J Cardiovasc Magn Res 2012;14:88.
68. White SK, Sado DM, Fontana M, et al. T1 mapping for myocardial extracellular volume measurement by CMR: bolus only versus primed infusion technique. J Am Coll Cardiol Img 2013;6: 955–62.
69. Mehta BB, Chen X, Bilchick KC, Salerno M, Epstein FH. Accelerated and navigator-gated look-locker imaging for cardiac t1 estimation (ANGIE): development and application to T1 mapping of the right ventricle. Magn Res Med 2015;73:150.
70. Weingärtner S, Roujol S, Akçakaya M, Basha TA, Nezafat R. Free-breathing multislice native myocardial T1 mapping using the slice-interleaved T1 (STONE) sequences. Magn Res Med 2015;74:115.
71. Mehta BB, Salerno M, Epstein FH. High-resolution three-dimensional ANGIE T1 mapping of the whole heart. J Cardiovasc Magn Res 2015;17:W4.
72. Kvernby S, Warntjes MJB, Haraldsson H, Carlhäll c-J, Engvall J, Ebbers T. Simultaneous three-dimensional myocardial T1 and T2 mapping in one breath hold with 3D-QALAS. J Cardiovasc Magn Res 2014;16:102.
73. Nordio G, Henningsson M, Chiribiri A, Villa ADM, Schneider T, Botnar RM. 3D myocardial T1 mapping using saturation recovery. J Magnet Res Img 2017;46:218.
74. Liu Y, Hamilton J, Rajagopalan S, Seiberlich N. Cardiac magnetic resonance fingerprinting: technical overview and initial results. J Am Coll Cardiol Img 2018;11:1837.
75. Hamilton JI, Jiang Y, Chen Y, et al. MR fingerprinting for rapid quantification of myocardial T1, T2, and proton spin density. Magn Res Med 2017;77:1446.
76. Hamilton JI, Jiang Y, Ma D, et al. Investigating and reducing the effects of confounding factors for robust T1 and T2 mapping with cardiac MR fingerprinting. Magn Res Img 2018;53: 40.
77. Shaw JL, Yang Q, Zhou Z, et al. Free-breathing, non-ECG, continuous myocardial T1 mapping with cardiovascular magnetic resonance Multitasking. Magn Res Med 2019;81:2450–63.
78. Bohnen S, Prüβner L, Vettorazzi E, et al. Stress T1-mapping cardiovascular magnetic resonance imaging and inducible myocardial ischemia. Clin Res Cardiol 2019:1.

## HIGHLIGHTS

- Mapping of myocardial T1 and ECV valves can provide noninvasive tissue characterization with powerful diagnostic, diminiscratory, and prognostic potential.
- Specific T1 and ECV values are dependent on several factors, including magnetic field strength, vendor, mapping technique, and sequence parameters.
- Each institution should develop and maintain a site-specific range of normal values.
- The field awaits the development of mapping techniques capable of whole-heart coverage, 3-dimensional datasets and free-breathing acquisition.

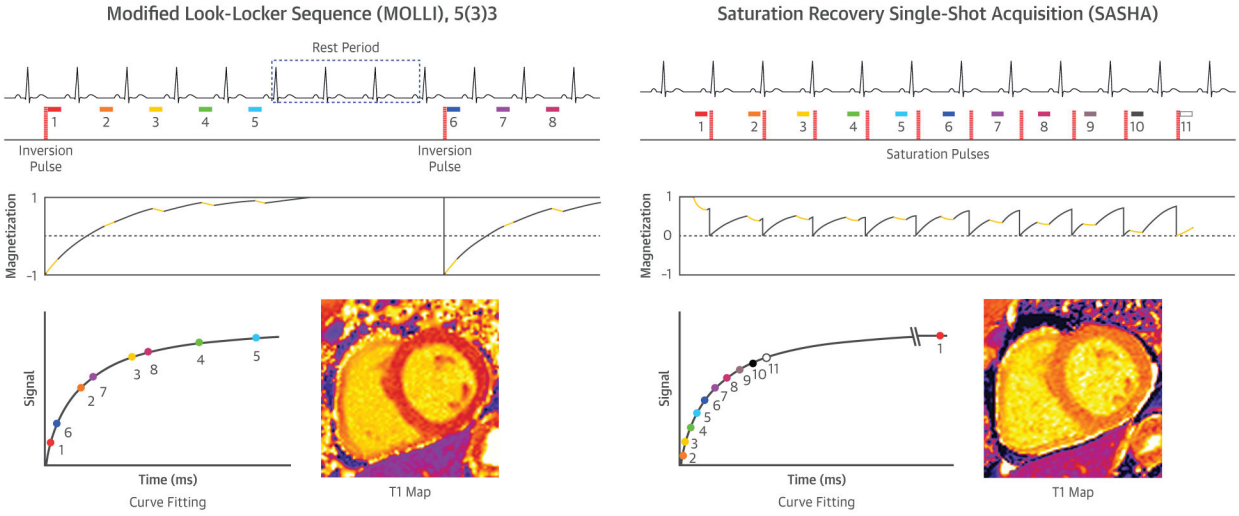


**FIGURE 1. T1 Mapping Involves Estimating the Recovery of Longitudinal Magnetization by Sampling the Magnetization at Various Points Along This Curve**

The 2 most common techniques for T1 mapping are inversion recovery (exemplified by MOLLI) and saturation recovery (exemplified by SASHA).

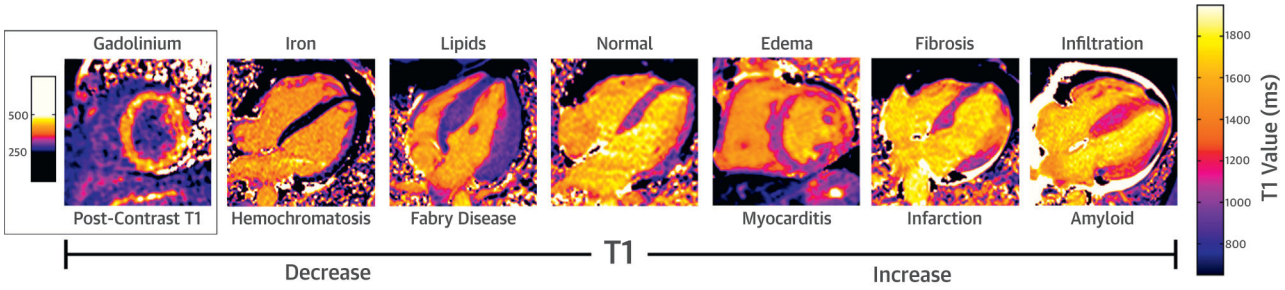


**FIGURE 2. Factors Affecting Native Myocardial T1**

Native T1 is decreased in the presence of iron and lipids. Native T1 is increased in the presence of edema, fibrosis, and myocardial infiltration.

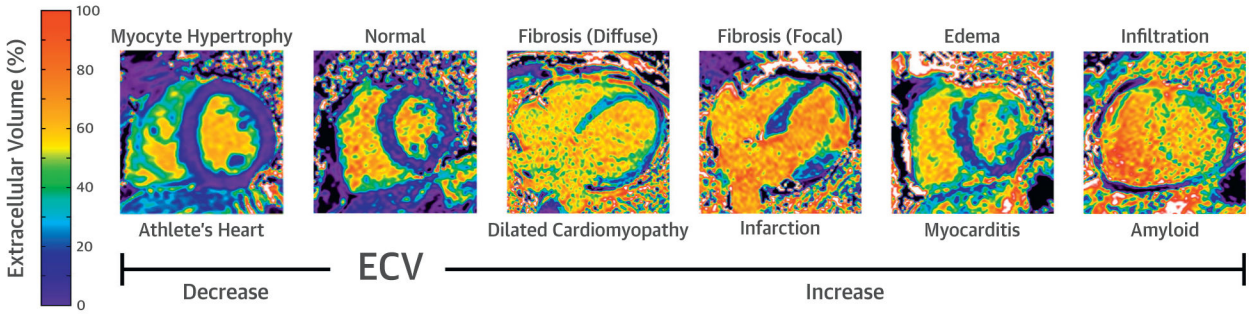


**FIGURE 3. Factors Affecting the Measurement of ECV Fraction**

ECV fraction can be decreased in the setting of myocardial infiltration, edema, and fibrosis (focal or diffuse). ECV is decreased in athletic remodeling resulting from an increase in the intracellular (myocyte) space, relative to the extracellular space. ECV = extracellular volume.

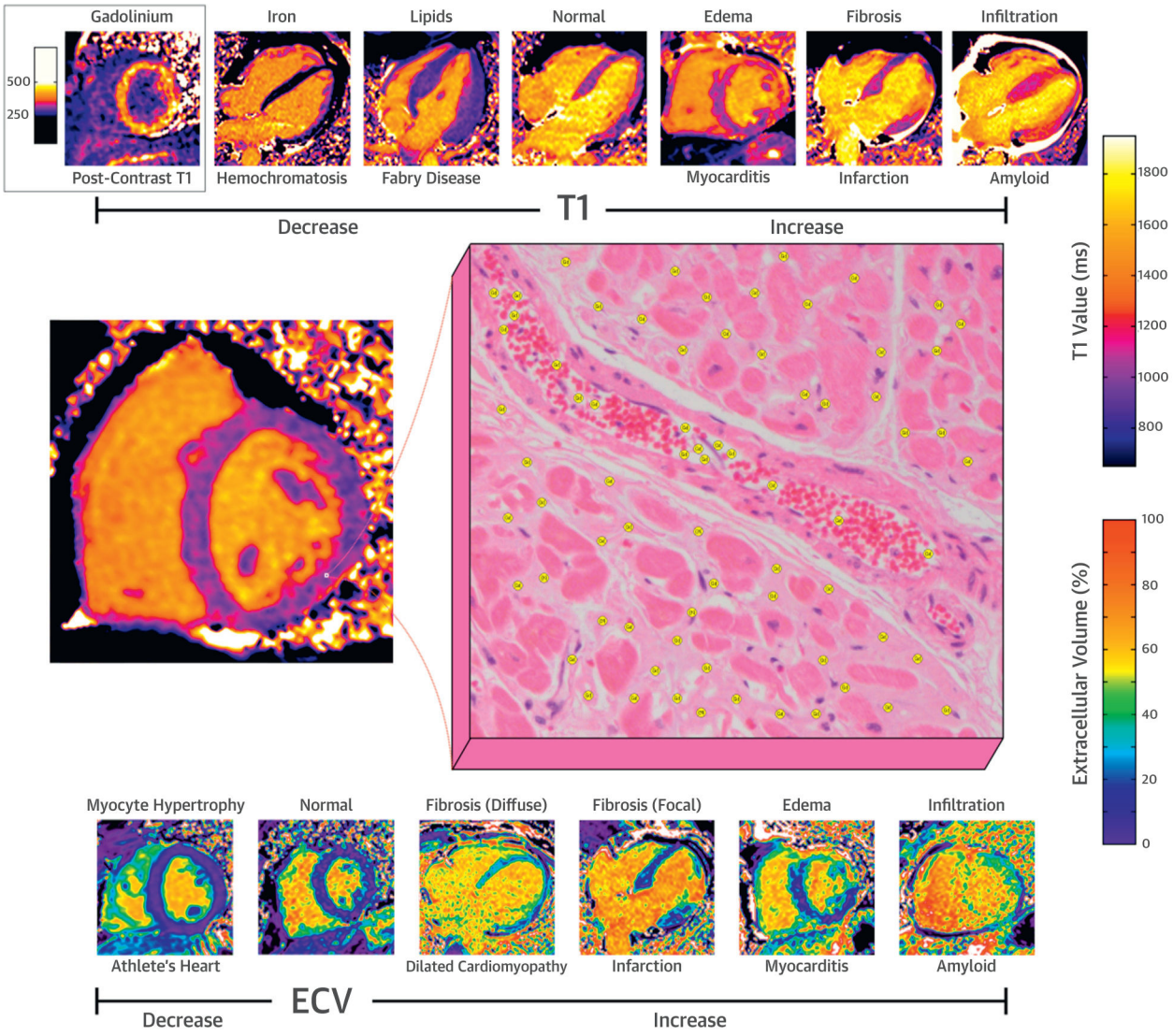


**CENTRAL ILLUSTRATION. Factors Affecting Myocardial T1 and ECV**

T1 and ECV mapping provide pixel-wise myocardial characterization. Components inside of each voxel include the intracellular space (e.g., myocytes, fibrocytes, blood cells), the plasma space, and the extravascular extracellular interstitial space. Changes in the components or size of these spaces are reflected by changes in the measured native T1 and ECV. ECV = extracellular volume.